Heteroanionic Ruddlesden-Popper ferroelectrics from anion order and octahedral tilts

Jaye K. Harada, ¹ Kenneth R. Poeppelmeier, ^{1, 2} and James M. Rondinelli^{1, *}

¹ Department of Materials Science and Engineering,
Northwestern University, Evanston, IL 60208, USA

² Department of Chemistry, Northwestern University, Evanston, IL 60208, USA

(Dated: September 20, 2021)

We describe a strategy to design ferroelectric heteroanionic materials based on the coupling of anion order and octahedral tilts in n=1 Ruddlesden-Popper structures, which allows noncentrosymmetric and polar compounds to arise from centrosymmetric anion ordered structures. We investigate the relative phase stabilities of the polymorphs of $\rm Sr_2ScO_3F$ and $\rm Ca_2ScO_3F$ derived from this coupling using electronic structure calculations. We find that large degrees of octahedral tilting can stabilize different anion orders derived from assembly of $[\rm ScO_5F]^{8-}$ octahedra. To further understand the link between octahedral tilting and anion order, we quantitatively separate the contributions of electrostatics and covalent interactions to the stability of tilts. We find that the tilts are driven primarily by covalent interactions and that local out-of-plane polar displacements, induced from the anion order, further stabilize the octahedral tilts through the pseudo-Jahn-Teller effect.

I. INTRODUCTION

The development of ferroic-based microelectronic components, such as non-volatile ferroelectric memory cells [1, 2], relies on advances in novel ferroelectric materials, i.e., materials whose spontaneous polarization is switchable through an external electric field. New mechanisms to induce ferroelectricity in known or novel compounds are therefore key to the development of better technologies. For example, the design and validation of alternative ferroelectric mechanisms such as improper [3] and hybrid improper ferroelectricity [4, 5] over proper ferroelectricity has expanded the design space for novel ferroelectric materials [6].

Designing ferroelectrics in ceramics has largely focused on homoanionic perovskite-derived oxide materials. In proper ferroelectrics such as BaTiO₃, the electronic polarization originates from off-centering of the Ti ion which is generally driven by the second-order Jahn-Teller or pseudo-Jahn-Teller (PJT) mechanism [7, 8] and stabilizes the off-centering of the Ti ion through covalent interactions [9, 10]. However, this interaction relies on d^0 transition metals in such materials, which severely limits the number of potential compounds and restricts routes to couple the electric polarization to a net magnetization. To facilitate coupling to magnetism and expand the available design space, improper and hybrid improper ferroelectric mechanisms can be used. They induce polarity through an anharmonic (multi-)mode coupling of polarization to zone-boundary modes such as octahedral tilts or rotations [11-14]. In hybrid improper ferroelectrics, the polarization is induced through antipolar displacements of chemically distinct A-site cations, which removes the reliance on d^0 transition metals and may allow for magnetoelectric coupling [15, 16]. This research led to the discovery of similar anharmonic multimode couplings that

induce polarization by coupling octahedral rotations to other types of distortions (e.g., Jahn-Teller, antiferroelectric modes, etc.) in both organic and inorganic perovskites and perovskite-derived phases [17–22]. These polarizations are all typically induced by the A-site cations or cation order.

Heteroanionic or multi-anion materials have emerged as an active area of research as one can leverage anion substitution to enhance and design new materials with functional properties, including those rooted in acentricity such as ferroelectricity, piezoelectricity, and second harmonic generation [23–25]. Several heteroanionic materials have been investigated for potential ferroelectricity, however many of their electronic polarizations originate from mechanisms observed in homoanionic materials. (Relaxor) ferroelectric behavior has been observed in SrTaO₂N in both epitaxial thin films and on the surface of bulk samples [26, 27]. Density functional theory (DFT) calculations and later measurements of the anion order [28] suggest that small domains of trans-type anion ordering with symmetry P4mm was the origin of the electric polarization. The polarization in that structure is driven by the pseudo-Jahn-Teller effect, which drives polar off-centering distortions of the Ta⁵⁺ within the trans-[TaO₄N₂] octahedra. The polar structure of BaWON₂ also originates from off-centering distortions, but its ferroelectricity is ambiguous [29].

Computational studies of oxynitrides have also predicted polar oxynitrides. LaTiO₂N is predicted to be polar under high compressive strain with possible switchable ferroelectricity, but the polarity originates from the off-centering distortions [30]. Ca₃Nb₂O₅N₂ is predicted to exhibit a polar structure, although the polarization originates from antipolar A-site displacements as in other homoanionic, hybrid improper n=2 Ruddlesden-Popper compounds [31]. Na₃MoO₃F₃ is a known polar oxyfluoride and has been investigated for switchable ferroelectricity [32]. However, the polarization arises from aligned dipoles formed from the [MoO₃F₃]³⁻ heteroleptic units, which would require large mass transport in order to switch the

^{*} jrondinelli@northwestern.edu

direction of the polarization.

Recently, the polar oxyfluoride, KNaNbOF₅, has found renewed interest as a potential ferroelectric [33, 34]. Unlike other known polar or ferroelectric heteroanionic compounds comprising oxygen and another main-group anion, the polarization arises from the coupling of in-phase and out-of-phase polyhedral rotations to a polar distortionantipolar displacements of the O and F anions [35]. Motivated by these studies on polar heteroanionic materials. herein we describe a strategy to find stable ferroelectric phases in heteroanionic materials. The coexistence of anion order and octahedral tilts generates a polarization in centrosymmetric (CS) anion ordered compounds. This method of coupling of anion rather than cation order to other displacive order parameters to generate polar structures was previously proposed in Ref. 36 for double pervoskites, however, the examination of these phase transitions was not pursued. It was also explored for a limited case of perovskite oxysulfides [37] and Aurivillius oxyfluorides [38].

Here, we examine the interactions between anion order and octahedral tilts in n = 1 Ruddlesden-Popper oxyfluorides with chemical formula A_2BO_3F and evaluate the relative energetics and driving forces to form the derivative phases through ab initio DFT calculations. We first enumerate the possible structures arising from the coupling of anion orders to octahedral tilts and determine which couplings generate polar (or noncentrosymmetric) phases where we find that only antipolar intralayer anion orders generate polar compounds from CS anion orders. Next, we use DFT calculations to evaluate the energy of these phases relative to their anion ordered structures in Sr₂ScO₃F and Ca₂ScO₃F. In Ca₂ScO₃F, the stabilization from the octahedral tilts are nearly great enough to switch the anion order from antipolar interlayer in Sr₂ScO₃F to antipolar intralayer in Ca₂ScO₃F. This finding suggests that the choice of A-site cations and octahedral tilts can change the relative stability of the anion orders. We then investigate the driving force for these rotations to better understand the microscopic origin of the anionorder-octahedral-tilt stabilization. We find that covalent metal-ligand interactions within the $[ScO_5F]^{8-}$ octahedron play a key role in stabilizing the octahedral tilts.

II. METHODS

All calculations were performed using DFT as implemented in the Vienna *ab initio* Simulation Package (VASP) [39, 40]. We used the generalized gradient approximation of the exchange correlation functional of Perdew, Burke, and Ernzerhof revised for solids (PBEsol) [41], as recommended for computational studies of oxyfluorides [42], and the projector augmented plane-wave (PAW) potentials [43] for the separation of core and valence electrons. The valence configurations used for the elements are as follows: $4s^24p^65s^2$ for Sr, $3s^23p^64s^2$ for Ca, $3p^64s^23d^1$ for Sc, $2s^22p^4$ for O, and $2s^22p^5$ for F. We used

a cutoff energy of 650 eV and a $6\times6\times3$ Monkhorst-Pack k-mesh [44] for structure relaxations and total energy calculations. Structure relaxations were converged by requiring forces to be less than $1\,\mathrm{meV}\,\mathring{\mathrm{A}}^{-1}$ on each atom and stresses of less than $10\,\mathrm{MPa}$ along each crystal axis. Phonon frequencies and eigenvectors were computed using the frozen phonon method. To ensure accurate phonon frequencies and eigenvectors across the Brillouin zone, $2\times2\times2$ supercells were used for all phonon-dispersion calculations. Phonon calculations were prepared and analyzed using the PHONOPY software package [45].

Symmetry-mode analyses of structures were carried out using the AMPLIMODES [46] and ISODISTORT [47, 48] software packages. The electronic polarization was calculated according to the Berry phase method and the modern theory of polarization [49, 50]. The procedure for the separation of interatomic force constants has been published previously and was followed here [51]. To evaluate the covalent interactions in the system, we computed the crystal orbital Hamiltonian populations (COHPs) using the LOBSTER code [52–55]. The COHP quantifies the orbital overlap in a given structure and projects these orbitals onto a particular atomic (or orbital) pairs (pCOHPs).

III. RESULTS AND DISCUSSION

A. Improper Anion-Ordered Ferroelectricity

1. Symmetry Analysis

We propose a chemical ordering form of improper ferroelectricity, which we refer to as improper anion-ordered ferroelectricity. Similar to the hybrid improper ferroelectricity, the mechanism active here relies on anharmonic multi-mode coupling to induce polar distortions in the compound. However, this mechanism relies on coupling an order parameter describing anion order to a displacive order parameter describing octahedral tilts, which makes it exclusive to heteroanionic materials and different from compounds where cation order facilitates broken inversion symmetry in the presence of nonpolar lattice distortions [4, 17, 22].

The main idea we follow is that a low-symmetry phase arises from distortions to an ideal high symmetry phase. Symmetry modes, which act as basis functions of irreducible representations or irreps of the space group of the ideal phase, then describe the symmetry breaking and serve as order parameters in the real or hypothetical phase transition used to "derive" the low-symmetry phase. The mechanical and permutation representations of these irreps may account independently or simultaneously for atomic displacements and atomic chemical ordering on different Wyckoff sites. As a result, there are interdependencies among the two representations that provide for the symmetry lowering through displacive or

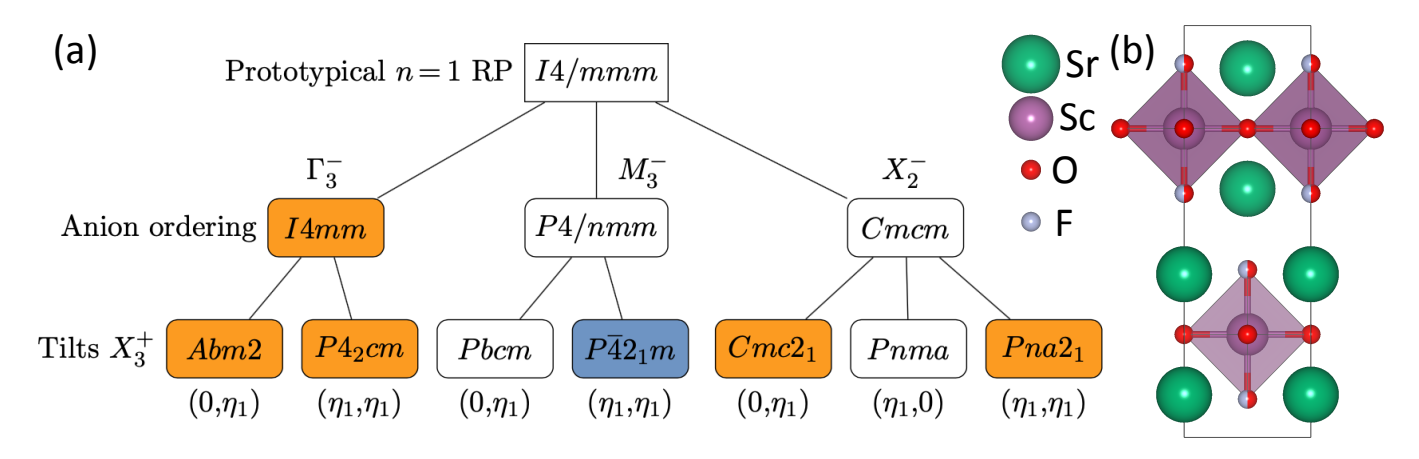


FIG. 1. (a) Group-subgroup relationships among anion ordered structures coupled to octahedral tilts. Each anion ordering (second row) is associated with an irrep of the (b) parent phase, n=1 RP with space group I4/mmm. The third row couples the anion order to an octahedral tilt, irrep X_3^+ , with the order parameter direction indicated below each space group label. Orange shaded space groups are polar and blue shaded space groups are nonpolar-noncentrosymmetric. Lines connecting space groups indicate that the phase transition is allowed to be continuous in Landau theory.

TABLE I. The effect of individual irreps on the Wyckoff sites of the ideal I4/mmm Ruddlesden-Popper A_2BX_4 compound due to anion ordering (O) and atomic displacements (D). The \times indicates that the irrep does not modify the specified Wyckoff site. Ligand sites X are either apical (ap) or equatorial (eq).

Species	Site	Γ_3^-	M_3^-	X_2^-	X_3^+
\overline{A}	4e	D	D	D	D
B	2a	D	D	D	×
X1 (ap)	4e	$_{\mathrm{D,O}}$	$_{\mathrm{D,O}}$	$_{\mathrm{D,O}}$	D
X2 (eq)	4c	D	D	×	D

order/disorder mechanisms in a physical phase transition. Fig. 1a illustrates this coexistence and/or coupling. Here the minimum set of irreps that describe out-of-phase octahedral tilts and common anion ordering in heteroleptic [BO₅F] octahedra [25] are combined into the ideal anion disordered $n = 1 A_2 BO_3 F$ Ruddlesden-Popper structure with I4/mmm symmetry (Fig. 1b), to produce lower symmetry derivative structures. The applied anion orders affects the ligand Wyckoff sites as given in Table I, where we demonstrate that these anion-order modes affect individual atomic sites by displacing them (D) and/or splitting the sites through chemical ordering (O). The chemical ordering component of these anion-order modes appear as the polar anion order, irrep Γ_3^- , in which the fluoride ion is exclusively located at the top apical ligand position; the antipolar interlayer anion ordering, irrep M_3^- , in which the fluoride ion switches between the top and bottom apical positions between adjacent perovskite layers; and the antipolar intralayer anion ordering, irrep X_2^- , in which the fluoride ion switches between the top and bottom positions within the same perovskite layer. Likewise, the ionic displacement component of these anion-order modes consists of local out-of-plane polar distortions of the B-cation site that are consistent with the type of anion order (i.e., the B cation moves towards the apical O in $[BO_5F]$ octahedra) as well as coordinated displacements of the A, X1, and X2 sites. The interlayer anion ordering appears to be the most commonly observed among synthesized anion ordered heteroanionic materials [56-62]. Polar anion order has also been observed [63, 64] whereas intralayer anion order has not been seen [25]. The octahedral tilts described by irrep X_3^+ always rotate about an in-plane axis and have two order parameter directions, $(0,\eta_1)$ or $(\eta_1,0)$ and (η_1,η_1) , which correspond to the octahedral tilts $a^-a^-c^0/a^-a^-c^0$ and $a^-b^0c^0/b^0a^-c^0$, respectively, in a modified Glazer notation [65], where the slash between the Glazer tilts indicates the octahedral tilt patterns for adjacent perovskite layers (Fig. 2a,b).

The derivative structures in the bottom row of Fig. 1a can be stabilized if the octahedral tilt modes, X_3^+ , are unstable in the anion ordered structure (second row of Fig. 1a). The lines connecting these phases implies a displacive phase transition could occur, in which the octahedral tilt modes condense to form the low symmetry phase. We show in the next section that most of these octahedral tilt modes are unstable in the anion ordered structures, however, here we focus on the implications of these changes for potential phase transitions. Fig. 1a shows that the polar anion order combined with the octahedral tilts always results in a polar structure. In contrast, the *interlayer* anion order and octahedral tilts produce centrosymmetric and nonpolar noncentrosymmetric structures. The *intralayer* anion order and octahedral tilts can produce polar structures; the polarization arises from the antipolar displacements of the anions. The structures along the $Cmc2_1$ phase transition pathway are shown in Supplementary Fig. S1 of Ref. 66, and indicate the polarization arises from all apical fluorides displacing along the [101] direction and the apical oxides displacing in the opposite [101] direction. Because the polarization arises

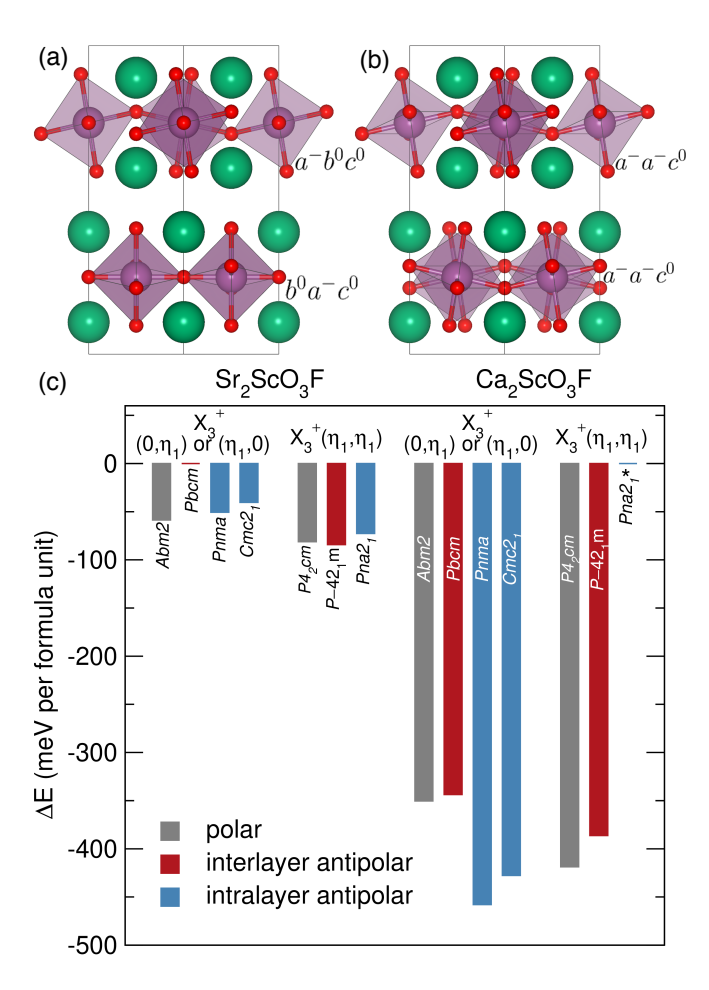


FIG. 2. Octahedral tilt patterns and energetics of the derivative structures relative to their anion ordered structures. The octahedral tilt patterns associated with the modes (a) X_3^+ (η_1 ,0) or (0, η_1) and (b) X_3^+ (η_1 , η_1). The tilts in Glazer notation are noted next to each perovskite layer. (c) The difference in energy ΔE between the relaxed derivative structures relative to the their anion ordered structures. The larger the difference, the more the derivative structure is stabilized by the indicated octahedral tilt pattern. The graph is separated into the two compounds, Sr_2ScO_3F and Ca_2ScO_3F , then further separated into the induced tilt pattern and anion orders (colors).

from small displacements, it may be switchable. This behavior is different from that in Na₃MoO₃F₃, whereby the polarization arises from aligned dipolar heteroleptic units [32].

The nature of the coupling can be understood through a polynomial expansion of the free energy change (ΔF) in terms of the symmetry allowed invariants comprising different order parameters. Using anion order (O), out-of-phase octahedral tilts (T), and the polarization (P) as the order parameters and the parent anion disordered n=1 Ruddlesden-Popper structure with I4/mmm symmetry serving as the reference structure, we obtain the following

free energy expansion:

$$\Delta F = \alpha_0 O^2 + \alpha_1 T^2 + \alpha_2 P^2 + \beta_0 O^4 + \beta_1 T^4 + \beta_2 P^4 + \gamma_0 O^2 T^2 + \gamma_1 T^2 P^2 + \gamma_2 P^2 O^2 + \delta OTP, \quad (1)$$

where $\alpha_i, \beta_i, \gamma_i$, and δ are the order parameter (coupling) coefficients. The stability of the polar phase originates from a delicate balance of energetically favorable and unfavorable couplings, which we will probe in the next section. For example, in hybrid improper materials, the trilinear term (δ) typically plays a significant role in stabilizing the polar structure, as the biquadratic couplings (γ_i) are typically energetically unfavorable [4, 12, 67]. Additionally, the homogeneous coefficients (i.e., α_i and β_i) also can be energetically unfavorable, so long as the biquadratic and/or trilinear term counterbalances the energy penalty and stabilizes the structure. If the free energy expansion is made with the antipolar intralayer anion ordered structure, then the change in translational periodicity causes the T mode to mix with P. As a result, a new order parameter P_T results, where the distinction between exclusively displacive and anion order parameters are lost. The new free-energy expansion then describes a proper ferroelectric with homogeneous quartic and quadratic terms: $\Delta F = \alpha P_T^2 + \beta P_T^4.$

2. Energetic Stability Analysis

To determine if the improper anion-order ferroelectricity mechanism occurs, we evaluate the energetics of the various phases obtained by combination of the aforementioned irreps. Note that we only use the displacive component of the anion-order mode O due to the difficulty in accurately calculating the energy of disordered anion solid-solution phases. So all reference energies are anion ordered phases. We choose Sr₂ScO₃F and Ca₂ScO₃F as models as the Sc^{3+} (d^0 configuration) ensures insulating character for all possible anion configurations. Sr₂ScO₃F has also been synthesized, with locally ordered [ScO₅F]⁸⁻ heteroleptic octahedra that are randomly oriented leading to the absence of long-range anion order [68]. The smaller ionic size of Ca compared to Sr also allows us to examine how different tilt patterns and tilt magnitudes, owing to the A-site cations differences, affect and contribute to phase stability [69].

Fig. 2c shows the relative energies of the relaxed tilted structures obtained from different order parameter directions of X_3^+ (Fig. 2a,b) for different anion ordered configurations (colored bars). Overall, the stability of the tilted polymorphs of Sr_2ScO_3F is weaker than the corresponding phases of Ca_2ScO_3F , with a few notable exceptions. The Sr_2ScO_3F Pbcm structure was not energetically favorable and the Ca_2ScO_3F $Pna2_1$ phase transforms into a different structure, indicated by the asterisk in Fig. 2c, albeit with the same symmetry. Therefore, we omit these two phases from further analysis. For both scandates, we also find that the $X_3^+(\eta_1,\eta_1) = a^-b^0c^0/b^0a^-c^0$ tilt

pattern tends to stabilize the structure more than the $X_3^+(\eta_1,0)=a^-a^-c^0/a^-a^-c^0$ tilts.

We first examine the anion-order-dependent octahedral tilt stability trends in the $\text{Ca}_2\text{ScO}_3\text{F}$ phases, because the variations are more obvious. The stability of the octahedral tilts is much greater in the intralayer anion ordered structures compared to the other anion orders. In the structures with $X_3^+(\eta_1,0)$ octahedral tilts, the tilts in the intralayer compounds are approximately $100\,\text{meV}$ more stable compared to the interlayer and polar compounds. The $X_3^+(\eta_1,0)$ tilts are more stable in the intralayer anion orders than the $X_3^+(\eta_1,\eta_1)$ tilts, which does not occur in $\text{Sr}_2\text{ScO}_3\text{F}$.

Control of octahedral tilts may be a viable method to tune the equilibrium anion order. By examining the stability of the anion ordered phases without rotations (Supplementary Table S1), we find the most stable anion order is the antipolar interlayer order (the relative energies are -117.4, -204.8, and 0 meV per formula unit for the polar, interlayer, and intralayer anion orders, respectively). When tilts are added to these structures, the tilts stabilize the intralayer anion order the most, but they are not sufficient to overcome the large initial energy difference between the interlayer and intralayer anion orders. However, we find that the ground state structure of Ca₂ScO₃F has intralayer anion order (Supplementary Table S1), indicating that although the octahedral tilts alone are unable to change the most stable anion order, they increase the energetic competition among competing anion orders adopted in Ca₂ScO₃F.

The stability of tilts with differing anion order is weaker in Sr₂ScO₃F. In contrast to Ca₂ScO₃F, the octahedral tilt stability of intralayer anion orders are less stable compared to their polar and interlayer counterparts, although the difference is much smaller, on the order of 10s of meV. Like Ca₂ScO₃F, the interlayer and polar anion orders compete more closely with one another compared to the intralayer anion ordered phases. The most stable anion order without octahedral tilts is the interlayer antipolar order and this does not change when calculating the equilibrium and ground state structures (Supplementary Table S2).

The change in anion order of the ground states structures of Sr₂ScO₃F and Ca₂ScO₃F from interlayer to intralayer, is notable. The stability of the octahedral tilts in Ca₂ScO₃F appears to be greater with intralayer anion ordering, although the origin of this behavior is not obvious. Likewise, the choice of A-site cation has a strong effect on the relative energetics of the system. To gain further insight into these problems, we further decompose the energetic contributions to the octahedral tilt stability.

B. Energetic Contributions Stabilizing Octahedral Tilts with Differing Anion Orders

The derivative structures compared to their parent phase have two main displacive mode contributions, as

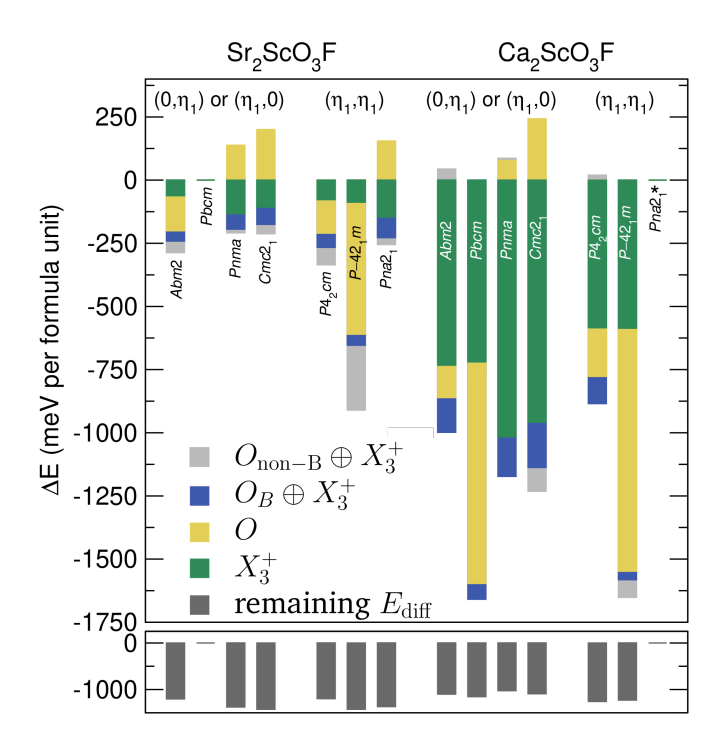


FIG. 3. Decomposed energetics of Sr_2ScO_3F and Ca_2ScO_3F relative to the undistorted anion ordered structures. The top panel divides the energy stabilization into the primary displacive mode contributions (anion order, O, and octahedral tilts, X_3^+) and the contribution from the coupling of these primary modes. The bottom panel takes the difference between the lattice energy of the relaxed structures and the unstrained structures with the primary modes shown here. The gain in energy in the bottom panel is primarily from fully symmetric ionic displacements and strain accommodation.

noted in Fig. 1a. The anion-order mode (O or Γ_3^- , M_3^- , and X_2^- for polar, interlayer, and intralayer anion orders, respectively) and the octahedral tilt modes X_3^+ . The final relaxed structures typically include one or two additional secondary modes; however, these modes do not alter the symmetry of the structure and do not contribute much to the energy (<10%). To gain further insight into the influence of anion order on the stability of octahedral tilts, we calculate the change in energy due to these primary modes, O and X_3^+ , both individually and coupled together, relative to the undisplaced anion ordered (i.e., appropriately O/F decorated) prototypical n=1 RP structure with rigid octahedra.

We obtain the symmetry-adapted modes of O and X_3^+ for each derivative structure, apply them to our undistorted anion ordered parent phase, and calculate their energies relative to the undistorted anion ordered parent to obtain the relative energy differences, ΔE_O and $\Delta E_{X_3^+}$. To gain further insight into which distortions couple favorably to the octahedral tilts, we separate the O displacements into two components, one containing only the B-site displacements (O_B , row B in Table I) and one containing all other displacements of the ions ($O_{\text{non-}B}$, rows A, X1, and X2 in Table I). We then couple them to

the octahedral tilts (i.e., $O_B \oplus X_3^+$ and $O_{\text{non-}B} \oplus X_3^+$), add them to the parent phase, calculate their energies relative to the parent phase, and subtract ΔE_O and $\Delta E_{X_3^+}$ from them to obtain the energetic change (gain or loss) from their coupling ($\Delta E_{O_B \oplus X_3^+}$ and $\Delta E_{O_{\text{non-}B} \oplus X_3^+}$).

These relative energies are shown in Fig. 3, with the different colors noting the individual or coupled contributions to the relative energy (ΔE). We find that the octahedral rotations, without any contribution from the anion ordered displacements ($\Delta E_{X_2^+}$, green bars in Fig. 3), stabilize the intralayer anion orders the most. The polar and interlayer anion orders follow next in stability and are in close competition with one another. The close competition between the polar and interlayer anion orders makes sense as there is essentially no difference between their anion orders within each perovskite layer, unlike the intralayer anion order. In the polar and interlayer anion orders, the F⁻ ion always sits on either the top or bottom apical ligand site, whereas the position of the F⁻ ion switches between the apical sites within a perovskite layer for the intralayer anion order.

The origin of the higher stability of the octahedral tilts in the intralayer compounds possibly originates in the alternating anion order in the perovskite layers. Our hypothesis is that in this ideal scenario, the electrostatic interactions of the apical sites, which move closer and further apart with the octahedral tilts, limit the degree of tilting. In the polar and interlayer compounds, the apical interactions are either O-O or F-F, and in the intralayer are always O-F. By using Coulomb's law, which gives an energy proportional to the product of the two point charges and their distance, the ratio of the average interaction of the apical sites in the polar and interlayer compounds compared to the intralayer compounds is 2.5: 2 = 1.25. This means that the destabilizing electrostatic interactions from the ligands are stronger in the polar and interlayer compounds, which is consistent with our DFT results.

Interestingly, displacements from the anion-order mode do not always stabilize the anion ordered structure (ΔE_O , yellow bars in Fig. 3). With intralayer anion ordering, displacements from $O(X_2^-)$ destabilize the structure. This likely explains why intralayer antipolar anion ordering has never been seen in synthesized heteroanionic RP compounds [25]. However, in the derivative structures, this destabilization is overcompensated by the stabilization gained from octahedral tilting and anharmonic coupling between O and X_3^+ . In Sr_2ScO_3F , the competition between these forces is close, but in Ca₂ScO₃F, the stabilizing forces far exceed the destabilizing ones, likely due to more acute octahedral tilting. The anion ordering displacements stabilize both the polar and interlayer anion orders, but the magnitude of the stabilization is several times larger in the interlayer anion ordered structures.

In all cases, coupling O and X_3^+ stabilizes the derivative structure. Our separation of the anion ordering mode O into the B-site only displacements (O_B) and all other displacements $(O_{\text{non-}B})$ helps us identify helps us identify

the origin of this stabilization when coupled to octahedral tilts. When octahedral tilts are coupled O_B (blue bars in Fig. 3), the structure is always more stable. Additionally, as the magnitude of the B-site displacements increase, $\Delta E_{O_B \oplus X_3^+}$ also increases in a nearly linear manner. As will be explained and quantified in the next section, the coupling creates unequal trans Sc-O_{eq} bond lengths in the [ScO₅F]⁸⁻ octahedra which stabilizes the structure through the PJT effect. Next, we consider all other ionic displacements in the anion-order mode $(O_{\text{non-}B})$ coupled to the octahedral tilts ($\Delta E_{O_{\text{non-}B} \oplus X_3^+}$, gray bars in the upper panel of Fig. 3). In most of the structures, this contribution is small and does not effect the relative energetics of the phases. There are a few exceptions, namely structures exhibiting $Cmc2_1$ and $P\bar{4}2_1m$ symmetry. This appears to be driven by the magnitude of the apical anion site displacements (4e), which makes sense as this will alter the bond lengths between Sc– O_{ap} and Sc–F and thus the strength of their covalent interactions. In general, it appears that the larger the apical anion site displacement, the larger the energetic gain.

In connecting this data back to Fig. 2, we first note that the ΔE values obtained are different. Data in Fig. 3 shows the energy change from specific modes without spontaneous lattice strains relative to the anion-ordered I4/mmm-like parent structure, whereas data in Fig. 2 shows the energy of the relaxed derivative structures relative to the relaxed anion ordered structures. The difference in energy between the fully relaxed derivative structures (i.e., Fig. 2) and the structures with only primary mode contributions (i.e., Fig. 3) are shown in the bottom panel of Fig. 3. This energy contains contributions from the aforementioned secondary modes, but is primarily composed of contributions from strain and fully symmetric ionic displacements (i.e., those transforming at Γ_1^+).

The data in Fig. 3 allows us to understand the connection between anion order and tilt stabilization. It clarifies that the trend in tilt stabilization is consistent between the Sr₂ScO₃F and Ca₂ScO₃F compounds, as intralayer anion ordering stabilizes the octahedral tilts the most in both compounds. The difference in the relative energetics of these phases likely lies in the energy scales and degree of rotations of the structures. In the Sr₂ScO₃F phases, the octahedral tilts are smaller and do not dominate the energetics, so competing factors have a much stronger effect on the overall energetics. In contrast, the degree of octahedral tilting in Ca₂ScO₃F is much greater owing to the small size of the A-site cation, thus the octahedral tilting dominates the relative energetics.

Through this analysis, we also learn how the $Cmc2_1$ and $Pna2_1$ phases are stabilized from terms in the Landau model (Equation 1). The homogeneous coupling constants (α_i and β_i) of X_3^+ are negative and are large in the case of Ca_2ScO_3F , so they likely contribute the most towards the stability of the polar phases. Interestingly, both the homogeneous coupling constants of O and P are energetically unfavorable (positive). In both

compounds, destabilization energy from P is small. However in $\operatorname{Sr}_2\operatorname{SCO}_3F$, the destabilization from O is similar in magnitude to X_3^+ , which means additional, energetically favorable couplings are necessary to stabilize the polar phase. The biquadratic coupling coefficients (γ_i) between O and X_3^+ are energetically favorable, which also helps stabilize the polar phase in $\operatorname{Sr}_2\operatorname{SCO}_3F$. The coupling between X_3^+ and P is also weakly energetically favorable. (The coupling between O and P was not probed.) The trilinear term appears to also further stabilize the phase as the hard mode, P (Γ_5^-), softens when the two primary modes O and X_3^+ condense (Supplementary Fig. S2). Now that we understand a significant factor in the stabilization of the polar phases in $\operatorname{Sr}_2\operatorname{ScO}_3F$ comes from the coupling of O and X_3^- , we examine the origin of the stabilization and quantify it.

C. Polar Displacements Stabilize Octahedral Tilts

In a typical homoanionic perovskite-derived material such as a transition metal oxide, sterics [70, 71] and covalent interactions [72–74] are known to drive rotations and tilts. Furthermore, octahedral tilts can compete with or facilitate local off-centering of cations due to the PJT effect [75, 76]. Because Ca₂ScO₃F and Sr₂ScO₃F are heteroanionic, we should also consider the role of the ligand electrostatic interactions (O²⁻ versus F⁻) on the octahedral tilt stability in the presence of steric, covalent, and cation off-centering.

To determine which interaction drives the octahedral tilts, we decompose the energy stabilization into its dipoledipole (electrostatic) and short-range contributions. The short-range contribution is essentially a catch-all term and encompasses all contributions which are not dipolar in nature, including steric and covalent interactions [51, 77]. We analyze the octahedral tilts modes relative to their relaxed anion ordered structures. Because this method is based on calculating the energetics from harmonic force constants, we use displacements normalized to 0.25 Å, which is why their energy differences do not exactly match those in Fig. 2. The separation of these contributions is shown in Table II and Table III for Sr₂ScO₃F and Ca₂ScO₃F, respectively. The polar off-centering distortions in BaTiO₃ are driven by dipole-dipole interactions which are nearly fully compensated by the short-range contribution [78]. Octahedral tilts are similarly driven by the PJT effect [72–74], so we may expect similar results here. In these heteoranionic materials we observe that the short-range contribution is the major driving force for the octahedral tilts. The dipole-dipole interactions either de-stabilize the octahedral tilts or stabilize them only by a small amount. The only exception to this is the $Cmc2_1$ and $P\overline{4}2_1m$ structures of Sr_2ScO_3F , in which the electrostatic contribution is about 20% of the total stabilization.

For comparison, this procedure was repeated for the $X_3^+(0,\eta_1)$ mode in the homoanionic prototypical n=1

TABLE II. Dipole-dipole (DD) and short-range (SR) contributions to the total (tot) change in energy in Sr₂ScO₃F structures with tilts relative to the anion ordered structures. All values are in meV.

	Abm2	Pbcm	Pnma	$Cmc2_1$	$P4_2cm$	$P\bar{4}2_1m$	$Pna2_1$
ΔE_{tot}	-22.5	_	-31.3	-28.3	-22.6	-23.4	-32.0
ΔE_{DD}	-0.9	_	5.6	-4.8	-1.2	-5.3	5.6
$\Delta E_{\rm SR}$	-21.6	_	-36.9	-23.5	-21.5	-18.1	-37.6

TABLE III. Dipole-dipole (DD) and short-range (SR) contributions to the total (tot) change in energy in Ca_2ScO_3F structures with tilts relative to the anion ordered structures. All values are in meV.

	Abm2	Pbcm	Pnma	$Cmc2_1$	$P4_2cm$	$P\bar{4}2_1m$	$Pna2_1$
ΔE_{tot}	-44.9	-48.4	-54.6	-51.3	-56.1	-56.8	_
$\Delta E_{\rm DD}$	2.3	11.3	8.1	9.8	-1.5	9.3	_
$\Delta E_{\rm SR}$	-47.2	-59.7	-62.7	-61.1	-54.6	-66.1	_

RP Sr₂SnO₄ (Supplementary Table S3). In this oxide, tilts driven by either ligand electrostatic effects or covalent interactions through the PJT are unlikely as all ligands are equivalent and the d orbitals are all occupied [72]. Nonetheless, the homoanionic case is very similar to the heteoranionic results as the short-range interaction stabilizes the tilt distortion more than the dipole-dipole interactions and these electrostatic interactions in fact act to destabilize the octahedral tilts. Although there should be no contribution from covalent interactions in the form of mixing ground and excited state wavefunctions, this approach does not allow us to fully disentangle the covalent interactions from steric interactions in the heteroanionic case. The covalent interaction would simply further stabilize the distortion through the short-range component. Therefore, from this data we can only conclude that electrostatic interactions do not drive the tilts in heteoranionic materials.

Aside from the charge difference from the anion substitution, the other major structural distinction from the prototypical homoanionic case is the local out-of-plane offcentering of Sc within the [ScO₅F]⁸⁻ octahedra from the anionic substitution. (Note that this is accompanied by additional displacements of the A-site cations and equatorial anions.) To clarify the role of the Sc displacement on the stability of the octahedral tilts, we freeze in rotations of varying amplitude into the anion ordered variants of the prototypical I4/mmm structure (i.e., the structures contain only the chemical ordering component of the anion-order mode) with and without the off-centering Sc displacements and calculate the relative energy changes (Fig. 4). The rotations are standardized to $X_3^+(\eta_1, \eta_1)$ and use the eigenvectors obtained from phonon calculations on a theoretical homoanionic analogue, Ca₂TiO₄. The magnitudes of the local out-of-plane off-centering displacements match those in the relaxed anion-ordered structures. For Sr₂ScO₃F, the magnitudes of the local

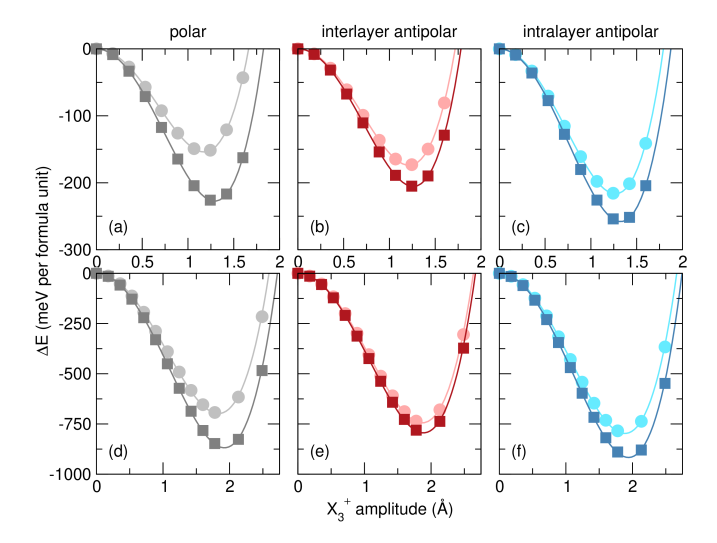


FIG. 4. Energetics of (a)-(c) Sr_2ScO_3F and (d)-(f) Ca_2ScO_3F with octahedral tilts in the presence and absence of Sc displacements due to the heteroleptic $[ScO_5F]^{8-}$ octahedron. The circles represent the prototypical I4/mmm structure and the squares represent the I4/mmm structure with the Sc displacements from the given composition and anion order. (a) and (d) have polar anion order, (b) and (e) have antipolar interlayer order, and (c) and (f) have antipolar intralayer order.

displacements are 0.23, 0.16, and 0.21 Å for the polar, interlayer, and intralayer anion orders, respectively. For Ca₂ScO₃F, the magnitudes of the local displacements are 0.23, 0.10, and 0.21 Å for the polar, interlayer, and intralayer anion orders, respectively.

We find that within each composition, the magnitude of the Sc displacements increases the stability of the octahedral tilts (Fig. 4). In all cases, the octahedral tilts are more stable in structures with local out-of-plane displacements (squares, darker lines) than in the structures without the Sc off-centering displacements (circles, lighter lines). The difference in energy minima between the Sr₂ScO₃F structures with and without the displacements are -73.3, -31.7, and -58.1 meV in the polar, antipolar interlayer, and antipolar intralayer structures, respectively, which scales with the size of the Sc displacement used in each anion order. Likewise, the energy differences for Ca₂ScO₃F are -170.5, -49.1, and -119.5 meV in the polar, antipolar interlayer, and antipolar intralayer, respectively.

We repeat this experiment with the all-oxide analogue, Ca_2TiO_4 to show that this effect is not unique to heteroanionic materials. Although Ti^{4+} can trigger an off-centering instability or a strong PJT effect, phonon calculations on I4/mmm Ca_2TiO_4 reveal that the off-centering distortion occurs along the in-plane direction [79] rather than an out-of-plane direction, as in these oxyfluorides. The layered structure of the oxide removes a driving force for out-of-plane polar distortions of the Ti^{4+} [80]. However, upon imposing the out-of-plane polar displacements and octahedral tilts into Ca_2TiO_4 , we find their coupling further stabilizes of the octahedral tilts in the

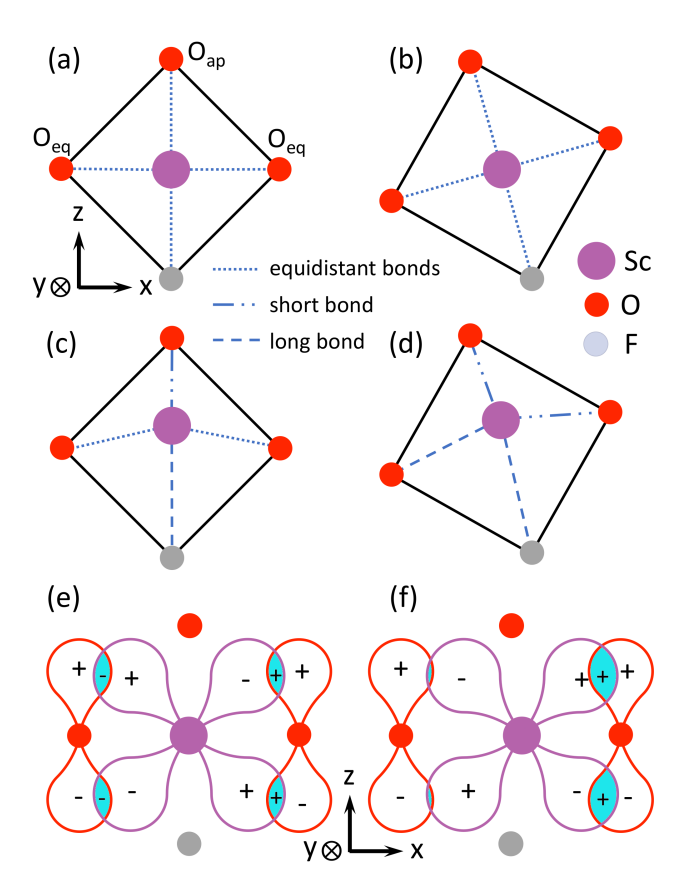


FIG. 5. (a-d) Illustrations of a $[ScO_5F]^{8-}$ octahedron showing how local polar displacements and octahedral tilts induce in-plane polar distortions into it. Octahedron without (a) and with (c) local polar displacements along the z axis. Corresponding structures with octahedral tilts are shown without (b) and with (d) polar Sc displacements. (e) and (f) illustrate how an in-plane polar displacement increases the Sc-O_{eq} π -bonding interactions between Sc d_{xz} and O_{eq} p_z orbitals. When Sc³⁺ is in the center of the octahedra (e), the Sc-O bonds are equidistant and thus, the net overlap between the π bonds is zero. When Sc³⁺ displaces along the x direction, the net overlap is non-zero. Panels (e) and (f) were adapted with permission from Ref. 10.

structure (Supplementary Fig. S3 in Ref. 66). The differences between the minimum energies of the structures with and without local Ti displacements are -15.2, -25.5, and -38.5 meV for the homoanionic polar, interlayer, and intralayer displacement patterns, respectively. The stability of these variants differs from the heteroanionic case because the magnitude of the Ti displacements used in ${\rm Ca_2TiO_4}$ are equivalent (0.18 Å). These trends indicate that anion order, or the pattern of out-of-plane polar displacements resulting from the anion order, have an influence on the tilt stability. However, the magnitude of the B-site displacement appears to have a much stronger affect on the tilt stability, based on Fig. 4 and the results in the next section.

The origin of this effect lies in a relatively simple geometric argument: the combination of octahedral tilts about an in-plane axis and static local polar displacements in a transverse out-of plane direction induces inplane B-cation displacements through a PJT effect. This combination of displacive modes is illustrated in Fig. 5a-d, where the Sc–O and Sc–F bond lengths within the xzplane of the [ScO₅F]⁸⁻ octahedron are shown without and with the octahedral rotations and Sc displacements. Without Sc displacements, the Sc-ligand bond lengths are all equal (Fig. 5a) and remain so with the octahedral tilt mode, X_3^+ , which involves equal but opposite directional displacements of the equatorial anions (O_{eq}) along the out-of-plane direction (Fig. 5b). Because the Sc displacement occurs along z to produce asymmetric apical Sc-O and Sc-F bond lengths (Fig. 5c), the nominally rigid rotation removes the equivalence between the trans $Sc-O_{eq}$ bonds and causes the bond lengths to become unequal (Fig. 5d). This asymmetry in the Sc-O_{eq} bond lengths increases the covalency from dp orbital mixing due to the PJT effect (compare the orbital overap in Fig. 5e,f). This is the same effect that stabilizes the polar displacements in BaTiO₃, where the mixing of occupied anion p orbitals and unoccupied metal d orbitals close to the Fermi level also occurs [9, 10, 81]. In this case, the enhanced covalency is mediated by the octahedral tilting that occurs among the heteroleptic units shown in Fig. 5e and f. When Sc is in the center of an octahedron, the positive orbital overlap of the Sc d_{xz} and O_{eq} p_z cancels the negative overlap so the net overlap is zero. When the Sc is displaced in the x-direction, the net overlap is non-zero.

The PJT effect is stronger when the states that are mixing are energetically close together. We first examine the molecular orbital diagram and density of states (DOS) for the Sc displaced structures to determine which interactions dominate. Since we substitute a F^- for an O^{2-} , the symmetry of the octahedra is no longer close to O_h (or $m\bar{3}m$ in Hermann-Mauguin notation), which means the d orbitals do not split into the typical e_q doublet and a t_{2g} triplet. Additionally, the significant difference in the electronegativities of F^- and O^{2-} splits the d orbitals within the e_q and t_{2q} states. The symmetry of the octahedra with one substituted site is C_{4v} (4mm) and we derive the molecular orbital diagram in Supplementary Fig. S3a, which matches the crystal field splitting of similar [MO₅X] octahedra [82–84]. The molecular orbital diagram predicts that the 3d orbitals (symmetry) from lowest to highest energy are ordered d_{xy} (b_2), { d_{xz} , d_{yz} } $(e), d_{x^2-y^2}(b_1), \text{ and } d_{z^2}(a_1), \text{ where the } d_{xz} \text{ and } d_{yz} \text{ or-}$ bitals are degenerate. The partial DOS for the anion ordered structures (Supplementary Fig. S3b) supports this interpretation, although the center of mass of the the d_{xy} bands is at higher energy than that of the degenerate (d_{xz},d_{yz}) orbitals, it does form the conduction band edge. For this reason, we consider only π -bonding interactions of the anions with the d_{xy} , d_{xz} , and d_{yz} orbital. Additionally, because the apical F 2p and O_{ap} states exhibit a_1 and b_1 symmetries, we do not consider the σ -type Sc– F and Sc-O_{ap} interactions. Thus, we only consider the

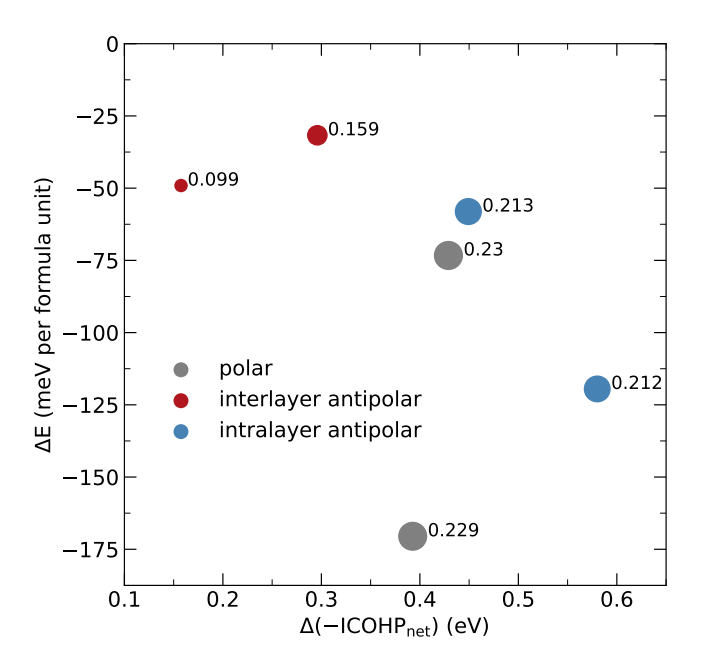


FIG. 6. Comparison of the energetic stabilization of octahedral tilts from Sc displacements, ΔE , to the increase in our covalency metric, $\Delta(-ICOHP_{net})$, from the same displacements. The magnitude of the Sc displacement is listed next to each data point and the marker size is proportional to the square of the magnitude of the Sc displacements.

following π Sc–O_{eq} interactions in our analysis: d_{xy} - p_x or p_y (dependent upon which axis O_{eq} is located), d_{xz} - p_z , and d_{yz} - p_z .

To quantify these changes in chemical bonding, we integrate the -pCOHP of the relevant π -bonding interactions (and obtain the -ICOHP, Supplementary Fig. S5) and take the difference between the Sc-O_{eq} bonds along the same axes, i.e., bonds which are trans to one another, to obtain the net overlap ($-ICOHP_{net}$). The difference is taken because the COHP does not account for the positive or negative phase of the orbital interactions. For consistency with the data in Fig. 4, we also take the difference between the net overlap of the structures with and without the Sc displacements to obtain the increase in covalency due to the out-of-plane off-centering and refer to it as $\Delta(-ICOHP_{net})$.

Fig. 6 plots the energetic gain of the octahedral tilts with the Sc displacements (from Fig. 4) against this increase in covalency due to the Sc displacements, along with the magnitude of the B-site displacement as the marker size. In general, the greater the increase in covalency, the more stabilizing the octahedral tilts. This trend is not perfectly linear, which may be due to missing secondary contributions to the overall change in energy or from A-site cations affecting the covalency of the Sc–O bonds via an inductive effect that is unaccounted for. Another possible missing energetic contribution is the change in covalency of the Sc–O_{ap} π -interaction, as discussed earlier. The choice of A-site cation can also influence the cova-

lency of the metal–anion bonds by reducing their bond formation through A-site s or p states hybridizing the occupied metal 3d states [74] (or occupied 2p states, in our case). However this seems unlikely, as "covalency-limiting" cations are generally those with large ionic size or high polarizability, and the largest outlier in Fig. 6 is from a Ca_2ScO_3F interlayer phase, which has a smaller ionic size and lower polarizability. We also plot the magnitude of the Sc displacements using the symbol size. In general, we also find an increase in the stability of the tilts (and, thus, the covalency) with the size of the Sc displacements, which is understandable as the Sc-Oeq bond lengths are dependent on the magnitude of this displacement.

From these analyses, we conclude that the octahedral tilts are driven through short-range interactions described by sterics or covalent interactions rather than electrostatic forces. The local out-of-plane polar displacements induced by the anion order drive and further stabilize the octahedral tilts through the PJT effect as the coupling of tilts and local polar distortions induces in-plane polar displacements in the heteroleptic octahedra.

IV. CONCLUSION

We described a novel mechanism for ferrolectricity in perovskite-derived heteroanionic materials, which we refer to as improper anion-order ferroelectricity. Anharmonic coupling between intralayer antipolar anion ordering and octahedral tilts generates polar displacements through antipolar displacement of O and F anions. We evaluated the feasibility of this mechanism through DFT calculations on $\rm Sr_2ScO_3F$ and $\rm Ca_2ScO_3F$ and found that intralayer anion ordering may be stabilized through large octahedral tilts. We also found that the driving force for octahedral tilts in these oxyfluorides appear to be no different than

the driving force in homoanionic materials—short-range interactions such as sterics and covalency appear to drive octahedral tilting. We also found that out-of-plane local polar displacements, driven by the anion substitution, further stabilize octahedral tilting through the PJT effect and the formation of unequal trans Sc-O_{eq} bonds. We showed that this stabilization is due to covalent effects through a COHP analysis and found that the magnitude of the B-site displacements serves as a useful descriptor for the relative stabilization effect of these out-of-plane local polar displacements. The link uncovered here between local polar displacements and octahedral tilts or rotations is intriguing and could have promising applications in multiferroic heteroanionic materials [85], as magnetic interactions could be tuned by rotations of the octahedra, which could be controlled through the magnitude of the transition metal cation displacements. We hope that these results spur interest in experimental synthesis and investigations into RP-type heteroanionic materials and anion order in complex transition metal compounds.

ACKNOWLEDGMENTS

J.K.H. would like to acknowledge Drs. Danilo Puggioni and Steven Flynn for helpful discussion, and Nathan Koocher for providing the crystal structure of Ca₂TiO₄ used in the analysis. J.K.H. and J.M.R. were supported by the National Science Foundation (NSF) Grant No. DMR-2011208. K.R.P. was supported by NSF DMR-1904701. Calculations were performed using the Extreme Science and Engineering Discovery Environment (XSEDE), which is supported by NSF Grant No. ACI-1548562, and use of the Center for Nanoscale Materials, an Office of Science user facility, was supported by the U.S. Department of Energy, Office of Science, Office of Basic Energy Sciences, under Contract No. DE-AC02-06CH11357.

O. Auciello, J. F. Scott, and R. Ramesh, The Physics of Ferroelectric Memories, Phys. Today 51, 22 (1998).

^[2] J. F. Scott, Ferroelectric Memories (Springer Berlin Heidelberg, 2000).

^[3] E. Bousquet, M. Dawber, N. Stucki, C. Lichtensteiger, P. Hermet, S. Gariglio, J.-M. Triscone, and P. Ghosez, Improper ferroelectricity in perovskite oxide artificial superlattices, Nature 452, 732 (2008).

^[4] N. A. Benedek and C. J. Fennie, Hybrid Improper Ferroelectricity: A Mechanism for Controllable Polarization-Magnetization Coupling, Phys. Rev. Lett. 106, 107204 (2011).

^[5] Y. S. Oh, X. Luo, F. T. Huang, Y. Wang, and S. W. Cheong, Experimental demonstration of hybrid improper ferroelectricity and the presence of abundant charged walls in (Ca,Sr)₃Ti₂O₇ crystals, Nat. Mater. 14, 407 (2015).

^[6] J. Young, A. Stroppa, S. Picozzi, and J. M. Rondinelli, Anharmonic lattice interactions in improper ferroelectrics for multiferroic design, J. Phys.: Condens. Matter 27, 283202 (2015).

^[7] J. K. Burdett, Use of the Jahn-Teller Theorem in Inorganic Chemistry, Inorg. Chem. 20, 1959 (1981).

^[8] I. B. Bersuker, Pseudo-Jahn-Teller Effect—A Two-State Paradigm in Formation, Deformation, and Transformation of Molecular Systems and Solids, Chem. Rev. 113, 1351 (2013).

^[9] R. E. Cohen, Origin of ferroelectricity in perovskite oxides, Nature 358, 136 (1992).

^[10] V. Polinger, P. Garcia-fernandez, and I. B. Bersuker, Pseudo Jahn – Teller origin of ferroelectric instability in BaTiO₃ type perovskites: The Green's function approach and beyond, Phys. B Phys. Condens. Matter 457, 296 (2015).

^[11] B. B. Van Aken, T. T. Palstra, A. Filippetti, and N. A. Spaldin, The origin of ferroelectricity in magnetoelectric YMnO₃, Nat. Mater. 3, 164 (2004).

^[12] J. M. Perez-Mato, P. Blaha, K. Schwarz, M. Aroyo, D. Orobengoa, I. Etxebarria, and A. García, Multiple instabilities in Bi₄Ti₃O₁₂: A ferroelectric beyond the soft-mode paradigm, Phys. Rev. B 77, 1 (2008).

- [13] N. A. Benedek, J. M. Rondinelli, H. Djani, P. Ghosez, and P. Lightfoot, Understanding ferroelectricity in layered perovskites: new ideas and insights from theory and experiments, Dalt. Trans. 44, 10543 (2015).
- [14] K. Xu, X.-Z. Lu, and H. Xiang, Designing new ferroelectrics with a general strategy, npj Quantum Mater. 2, 1 (2017).
- [15] J. M. Rondinelli and C. J. Fennie, Octahedral Rotation-Induced Ferroelectricity in Cation Ordered Perovskites, Adv. Mater. 24, 1961 (2012).
- [16] A. T. Mulder, N. A. Benedek, J. M. Rondinelli, and C. J. Fennie, Turning ABO₃ Antiferroelectrics into Ferroelectrics: Design Rules for Practical Rotation-Driven Ferroelectricity in Double Perovskites and A₃B₂O₇ Ruddlesden-Popper Compounds, Adv. Funct. Mater. 23, 4810 (2013).
- [17] L. Bellaiche and J. Íñiguez, Universal collaborative couplings between oxygen-octahedral rotations and antiferroelectric distortions in perovskites, Phys. Rev. B 88, 014104 (2013).
- [18] N. A. Benedek, Origin of ferroelectricity in a family of polar oxides: The Dion-Jacobson phases, Inorg. Chem. 53, 3769 (2014).
- [19] H. J. Zhao, J. Íñiguez, W. Ren, X. M. Chen, and L. Bellaiche, Atomistic theory of hybrid improper ferroelectricity in perovskites, Phys. Rev. B 89, 1 (2014).
- [20] H. J. Zhao, L. Bellaiche, X. M. Chen, and J. Íñiguez, Improper electric polarization in simple perovskite oxides with two magnetic sublattices, Nat. Commun. 8, 1 (2017).
- [21] J. Young, E. J. Moon, D. Mukherjee, G. Stone, V. Gopalan, N. Alem, S. J. May, and J. M. Rondinelli, Polar Oxides without Inversion Symmetry through Vacancy and Chemical Order, J. Am. Chem. Soc. 139, 2833 (2017).
- [22] H. L. Boström, M. S. Senn, and A. L. Goodwin, Recipes for improper ferroelectricity in molecular perovskites, Nat. Commun. 9, 1 (2018).
- [23] H. Kageyama, K. Hayashi, K. Maeda, J. P. Attfield, Z. Hiroi, J. M. Rondinelli, and K. R. Poeppelmeier, Expanding Frontiers in Materials Chemistry and Physics with Multiple Anions, Nat. Commun. 9, 772 (2018).
- [24] Y. Kobayashi, Y. Tsujimoto, and H. Kageyama, Property Engineering in Perovskites via Modification of Anion Chemistry, Annu. Rev. Mater. Res. 48, 303 (2018).
- [25] J. K. Harada, N. Charles, K. R. Poeppelmeier, and J. M. Rondinelli, Heteroanionic Materials by Design: Progress Toward Targeted Properties, Adv. Mater. 31, 1805295 (2019).
- [26] D. Oka, Y. Hirose, H. Kamisaka, T. Fukumura, K. Sasa, S. Ishii, H. Matsuzaki, Y. Sato, Y. Ikuhara, and T. Hasegawa, Possible ferroelectricity in perovskite oxynitride SrTaO₂N epitaxial thin films, Sci. Rep. 4, 4987 (2015).
- [27] S. Kikkawa, S. Sun, Y. Masubuchi, Y. Nagamine, and T. Shibahara, Ferroelectric Response Induced in cis-Type Anion Ordered SrTaO₂N Oxynitride Perovskite, Chem. Mater. 28, 1312 (2016).
- [28] D. Oka, Y. Hirose, F. Matsui, H. Kamisaka, T. Oguchi, N. Maejima, H. Nishikawa, T. Muro, K. Hayashi, and T. Hasegawa, Strain Engineering for Anion Arrangement in Perovskite Oxynitrides, ACS Nano 11, 3860 (2017).
- [29] J. Oró-Solé, I. Fina, C. Frontera, J. Gàzquez, C. Ritter, M. Cunquero, P. Loza-Alvarez, S. Conejeros, P. Alemany,

- E. Canadell, J. Fontcuberta, and A. Fuertes, Engineering Polar Oxynitrides: Hexagonal Perovskite BaWON₂, Angew. Chem. Int. Ed. **59**, 18395 (2020).
- [30] N. Vonrüti and U. Aschauer, Anion order and spontaneous polarization in latio₂N oxynitride thin films, Phys. Rev. Lett. 120, 046001 (2018).
- [31] G. Gou, M. Zhao, J. Shi, J. K. Harada, and J. M. Rondinelli, Anion Ordered and Ferroelectric Ruddlesden-Popper Oxynitride Ca₃Nb₂N₂O₅ for Visible-Light-Active Photocatalysis, Chem. Mater. 32, 2815 (2020).
- [32] F. J. Brink, L. Norén, D. J. Goossens, R. L. Withers, Y. Liu, and C.-N. N. Xu, A combined diffraction (XRD, electron and neutron) and electrical study of Na₃MoO₃F₃, J. Solid State Chem. 174, 450 (2003).
- [33] M. Holland, N. Charles, J. M. Rondinelli, and K. R. Poeppelmeier, Reconstructive Transitions from Rotations of Rigid Heteroanionic Polyhedra, J. Am. Chem. Soc. 138, 11882 (2016).
- [34] P.-H. Chien, J. K. Harada, H. Liu, S. Patel, C. Huang, J. M. Rondinelli, K. R. Poeppelmeier, and Y.-Y. Hu, Microscopic Insights into the Reconstructive Phase Transition of KNaNbOF₅ with ¹⁹F NMR Spectroscopy, Chem. Mater. 32, 5715 (2020).
- [35] A. K. Mishra, M. R. Marvel, K. R. Poeppelmeier, and U. V. Waghmare, Competing cation-anion interactions and noncentrosymmetry in metal oxide-fluorides: A firstprinciples theoretical study, Cryst. Growth Des. 14, 131 (2014).
- [36] N. Charles, R. J. Saballos, and J. M. Rondinelli, Structural Diversity from Anion Order in Heteroanionic Materials, Chem. Mater. 30, 3528 (2018).
- [37] G. Pilania, A. Ghosh, S. T. Hartman, R. Mishra, C. R. Stanek, and B. P. Uberuaga, Anion order in oxysulfide perovskites: origins and implications, npj Comput. Mater. 6, 71 (2020).
- [38] A. T. Giddings, E. A. S. Scott, M. C. Stennett, D. C. Apperley, C. Greaves, N. C. Hyatt, and E. E. Mc-Cabe, Symmetry and the Role of the Anion Sublattice in Aurivillius Oxyfluoride Bi₂TiO₄F₂, Inorg. Chem. 10.1021/acs.inorgchem.1c01933 (2021).
- [39] G. Kresse and J. Furthmüller, Efficient Iterative Schemes for Ab Initio Total-Energy Calculations Using a Plane-Wave Basis Set, Phys. Rev. B 54, 11169 (1996).
- [40] G. Kresse and J. Furthmüller, Efficiency of ab-initio total energy calculations for metals and semiconductors using a plane-wave basis set, Comput. Mater. Sci. 6, 15 (1996).
- [41] J. P. Perdew, A. Ruzsinszky, G. I. Csonka, O. A. Vydrov, G. E. Scuseria, L. A. Constantin, X. Zhou, and K. Burke, Restoring the Density-Gradient Expansion for Exchange in Solids and Surfaces, Phys. Rev. Lett. 100, 136406 (2008).
- [42] N. Charles and J. M. Rondinelli, Assessing Exchange-Correlation Functional Performance for Structure and Property Predictions of Oxyfluoride Compounds From First Principles, Phys. Rev. B 94, 174108 (2016).
- [43] P. E. Blöchl, Projector Augmented-Wave Method, Phys. Rev. B 50, 17953 (1994).
- [44] H. J. Monkhorst and J. D. Pack, Special Points for Brillouin-Zone Integrations, Phys. Rev. B 13, 5188 (1976).
- [45] A. Togo and I. Tanaka, First principles phonon calculations in materials science, Scr. Mater. 108, 1 (2015).
- [46] D. Orobengoa, C. Capillas, M. I. Aroyo, and J. M. Perez-Mato, AMPLIMODES: symmetry-mode analysis on the Bilbao Crystallographic Server, J. Appl. Crystallogr. 42,

- 820 (2009).
- [47] H. T. Stokes, D. M. Hatch, and B. J. Campbell, ISODIS-TORT
- [48] B. J. Campbell, H. T. Stokes, D. E. Tanner, and D. M. Hatch, ISODISPLACE: A Web-Based Tool for Exploring Structural Distortions, J. Appl. Crystallogr. 39, 607 (2006).
- [49] R. D. King-Smith and D. Vanderbilt, Theory of polarization of crystalline solids, Phys. Rev. B 47, 1651 (1993).
- [50] N. A. Spaldin, A beginner's guide to the modern theory of polarization, J. Solid State Chem. 195, 2 (2012).
- [51] X. Gonze, J. C. Charlier, D. C. Allan, and M. P. Teter, Interatomic force constants from first principles: The case of α-quartz, Phys. Rev. B 50, 13035 (1994).
- [52] R. Dronskowski and P. E. Blöchl, Crystal orbital hamilton populations (COHP). Energy-resolved visualization of chemical bonding in solids based on density-functional calculations, J. Phys. Chem. 97, 8617 (1993).
- [53] V. L. Deringer, A. L. Tchougréeff, and R. Dronskowski, Crystal orbital Hamilton population (COHP) analysis as projected from plane-wave basis sets, J. Phys. Chem. A 115, 5461 (2011).
- [54] S. Maintz, V. L. Deringer, A. L. Tchougréeff, and R. Dronskowski, Analytic projection from plane-wave and PAW wavefunctions and application to chemical-bonding analysis in solids, J. Comput. Chem. 34, 2557 (2013).
- [55] S. Maintz, M. Esser, and R. Dronskowski, Efficient rotation of local basis functions using real spherical harmonics, Acta Phys. Pol. B 47, 1165 (2016).
- [56] R. L. Needs and M. T. Weller, Synthesis and Structure of Ba₂InO₃F: Oxide/Fluoride Ordering in a New K₂NiF₄ Superstructure, J. Chem. Soc. Chem. Commun., 353 (1995).
- [57] R. L. Needs, M. T. Weller, U. Scheler, and R. K. Harris, Synthesis and Structure of Ba₂InO₃X (X = F, Cl, Br) and Ba₂ScO₃F; Oxide/Halide Ordering in K₂NiF₄-Type Structures, J. Mater. Chem. 6, 1219 (1996).
- [58] G. S. Case, A. L. Hector, W. Levason, R. L. Needs, M. F. Thomas, and M. T. Weller, Syntheses, powder neutron diffraction structures and Mössbauer studies of some complex iron oxyfluorides: Sr₃Fe₂O₆F_{0.87}, Sr₂FeO₃F and Ba₂InFeO₅F_{0.68}, J. Mater. Chem. 9, 2821 (1999).
- [59] S. M. Loureiro, C. Felser, Q. Huang, and R. J. Cava, Refinement of the Crystal Structures of Strontium Cobalt Oxychlorides by Neutron Powder Diffraction, Chem. Mater. 12, 3181 (2000).
- [60] A. L. Hector, J. A. Hutchings, R. L. Needs, M. F. Thomas, and M. T. Weller, Structural and Mössbauer Study of Sr₂FeO₃X (X = F, Cl, Br) and the Magnetic Structure of Sr₂FeO₃F, J. Mater. Chem. 11, 527 (2001).
- [61] C. S. Knee, A. A. Zhukov, and M. T. Weller, Crystal Structures and Magnetic Properties of the Manganese Oxide Chlorides Sr₂MnO₃Cl and Sr₄Mn₃O_{8-y}Cl₂, Chem. Mater. 14, 4249 (2002).
- [62] Y. Tsujimoto, K. Yamaura, and T. Uchikoshi, Extended Ni(III) Oxyhalide Perovskite Derivatives: Sr₂NiO₃X (X = F, Cl), Inorg. Chem. **52**, 10211 (2013).
- [63] R. Marchand, R. Pastuszak, and Y. Laurent, Structure Cristalline de Nd₂AlO₃N. Détermination de L'ordre Oxygéne-Azote par Diffraction de Neutrons, Rev. Chim. Miner. 19, 684 (1982).
- [64] F. Cheviré, A. Pallu, E. Ray, and F. Tessier, Characterization of Nd₂AlO₃N and Sm₂AlO₃N Oxynitrides Synthesized by Carbothermal Reduction and Nitridation, J.

- Alloys Compd. 509, 5839 (2011).
- [65] A. M. Glazer, The classification of tilted octahedra in perovskites, Acta Crystallogr. Sect. B: Struct. Crystallogr. Cryst. Chem. 28, 3384 (1972).
- [66] See Supplemental Material at http://link.aps.org/supplemental/10.1103/X.XXX.X for the homoanionic I4/mmm to heteroanionic Cmc2₁ phase transition pathway; calculated Berry phase polarization for the polar phases; the relative energies of the anion ordered phases and their equilibrium structures; confirmation the stabilizing trilinear term; separation of force constants for Sr₂SnO₄; relative energies of Ca₂TiO₄ with varying octahedral tilts and B-site displacement patterns; molecular orbital diagram of [ScO₅F] octahedra and the partial density of states of the relaxed anion ordered phases.
- [67] U. Petralanda and I. Etxebarria, Structural instabilities and sequence of phase transitions in SrBi₂Nb₂O₉ and SrBi₂Ta₂O₉ from first principles and Monte Carlo simulations, Phys. Rev. B 91, 184106 (2015).
- [68] Y. Y. Wang, K. Tang, B. Zhu, D. Wang, Q. Hao, and Y. Y. Wang, Synthesis and Structure of a New Layered Oxyfluoride Sr₂ScO₃F with Photocatalytic Property, Mater. Res. Bull. 65, 42 (2015).
- [69] We attempted to synthesize both compounds and were successful at reproducing the synthesis of Sr₂ScO₃F, however we were unable to synthesize Ca₂ScO₃F through solid state and ion-exchange methods. Convex hull calculations indicate that both compounds sit above the hull, the ground states of the compounds are at a distance of 9 meV per atom for Sr₂ScO₃F and 67 meV per atom for Ca₂ScO₃F.
- [70] I. D. Brown, Chemical and Steric Constraints in Inorganic Solids, Acta Crystallogr. Sect. B: Struct. Sci. 48, 553 (1992).
- [71] P. M. Woodward, Octahedral Tilting in Perovskites. II. Structure Stabilizing Forces, Acta Crystallogr. Sect. B: Struct. Sci. 53, 44 (1997).
- [72] P. Garcia-Fernandez, J. A. Aramburu, M. T. Barriuso, and M. Moreno, Key Role of Covalent Bonding in Octahedral Tilting in Perovskites, J. Phys. Chem. Lett. 1, 647 (2010).
- [73] P. Aguado-Puente, P. García-Fernández, and J. Junquera, Interplay of couplings between antiferrodistortive, ferroelectric, and strain degrees of freedom in monodomain PbTiO₃/SrTiO₃ superlattices, Phys. Rev. Lett. 107, 1 (2011).
- [74] A. Cammarata and J. M. Rondinelli, Covalent dependence of octahedral rotations in orthorhombic perovskite oxides, J. Chem. Phys. 141, 114704 (2014).
- [75] N. A. Benedek and C. J. Fennie, Why Are There So Few Perovskite Ferroelectrics?, J. Phys. Chem. C 117, 13339 (2013).
- [76] Y. Mochizuki, T. Nagai, H. Shirakuni, A. Nakano, F. Oba, I. Terasaki, and H. Taniguchi, Coexisting Mechanisms for the Ferroelectric Phase Transition in Li₂SrNb₂O₇, Chem. Mater. 33, 1257 (2021).
- [77] P. Ghosez, E. Cockayne, U. V. Waghmare, and K. M. Rabe, Lattice dynamics of BaTiO₃, PbTiO₃, and PbZrO₃: A comparative first-principles study, Phys. Rev. B 60, 836 (1999).
- [78] P. Ghosez, X. Gonze, and J.-P. Michenaud, Coulomb interaction and ferroelectric instability of BaTiO₃, Europhys. Lett. 33, 713 (1996).
- [79] N. Z. Koocher, L.-F. Huang, and J. M. Rondinelli, Negative thermal expansion in the ruddlesden-popper calcium

- titanates, Phys. Rev. Materials 5, 053601 (2021).
- [80] T. Birol, N. A. Benedek, and C. J. Fennie, Interface Control of Emergent Ferroic Order in Ruddlesden-Popper $\mathrm{Sr}_{n+1}\mathrm{Ti}_n\mathrm{O}_{3n+1},$ Phys. Rev. Lett. 107, 257602 (2011).
- [81] D. Hickox-Young, D. Puggioni, and J. M. Rondinelli, Persistent polar distortions from covalent interactions in doped BaTiO₃, Phys. Rev. B 102, 1 (2020).
- [82] C. J. Ballhausen and H. B. Gray, The Electronic Structure of the Vanadyl Ion, Inorg. Chem. 1, 111 (1962).
- [83] J. R. Winkler and H. B. Gray, Electronic Absorption and Emission Spectra of Dioxorhenium(V) Complexes. Characterization of the Luminescent 3Eg State, Inorg. Chem. **24**, 346 (1985).
- [84] K. Meyer, J. Bendix, E. Bill, T. Weyhermüller, and K. Wieghardt, Molecular and Electronic Structure of Nitridochromium(V) Complexes with Macrocyclic Amine Ligands, Inorg. Chem. 37, 5180 (1998).
- [85] S. T. Hartman, S. B. Cho, and R. Mishra, Multiferroism in Iron-Based Oxyfluoride Perovskites, Inorg. Chem. 57, 10616 (2018).